Large-deviations of the Basin Stability of power grids

Yannick Feld[1, a)] and Alexander K. Hartmann[1, b)]
Institut für Physik, Carl von Ossietzky Universität Oldenburg, 26111 Oldenburg, Germany

(Dated: September 30, 2019)

Energy grids play an important role for modern society. In recent years there was a shift from using few central power sources to using many small power sources, due to efforts to increase the percentage of renewable energies. Therefore the properties of extremely stable and unstable networks are of interest.

In this paper distributions of the basin stability, a nonlinear measure to quantify the ability of a power grid to recover from perturbations, and its correlations with other measurable quantities, namely diameter, flow backup capacity, power-sign ratio, universal order parameter, biconnected component, clustering coefficient, two core, and leafs are studied. The energy grids are modeled by an Erdős-Rényi random graph ensemble and a small-world graph ensemble, where the latter is defined in such a way, that it does not exhibit dead ends. Using large deviation techniques, we reach very improbable power grids that are extremely stable as well as ones that are extremely unstable, respectively. The $1/t$-algorithm, a variation of Wang-Landau, which does not suffer from error saturation, and additional entropic sampling is used to achieve good precision even for very small probabilities ranging over eight decades.

Power grids, and therefore their stability, are of utmost importance for our modern society. A possible way to characterize the stability of power grids against perturbations is the nonlinear *basin stability* that was introduced in recent years. We now use a large deviation approach to investigate the probability density function of the basin stability, even for very small probabilities, for two different network ensembles. We are able to investigate the significance of static measurable quantities on the dynamic stability by measuring their correlations to the basin stability even for very improbable realizations of grids.

I. INTRODUCTION

Stability of complex systems[1,2] is an ubiquitous phenomenon which is an essential property of many natural and engineered systems on various length and time scales like the solar system,[3] ecological communities,[4,5] or gene networks.[6] Technological networks are crucial for the functioning of modern societies. Here one is interested in designing them in order to, first, fulfill the desired task in the standard case, but also such that they are resilient against fluctuations and failures. Thus, in contrast to natural systems, which are shaped by biological and physical evolution, technological networks can and have to be engineered to reach an optimum behavior. During recent years in particular energy grids came into the focus of research in engineering, computer science and statistical physics because of the ongoing change of the composition of the energy sources. Due to ongoing climate change, carbon-based energy resources have to be decreased.[7,8] Thus, more and more decentralized renewable energy sources become part of the grid, replacing centralized power generation of fossil fuel or nuclear power plants. This leads to a lot of challenges concerning grid topology and stability.[9] Instabilities, even originating on a small scale, can lead to failures and even cascading failures, i.e., large scale blackouts.[10]

Several different approaches to model power grids[11] exists. Viewed in an abstract way, a power grid is a general transport model, where some capacity for transporting the entity of interest has to be provided.[12–15] If one is not interested in the dynamics of power grids, one can just use Kirchoffs equations and study the power flow in the steady state.[16] Here one can study networks with respect to the (static) so called $N-1$ stability, which means that the electrical grid should provide enough transport capacity to compensate single line (or node) failures.[17]

If one is also interested in studying dynamic properties, e.g., resilience against fluctuations in time, one has to consider more elaborate models. By generalizing the *swing equation*[11,18] of a synchronous machine to small networks, Filatrella, Nielsen and Pedersen arrived[19] at a model similar to the Kuramoto model.[20] The dynamics of the oscillators i is here governed by the phase angles θ_i and influenced through the couplings of the oscillators. This model stimulated many studies in the field of power grids. In Ref. 21 the synchronization of this dynamical model on the topology of the power grid of the United Kingdom (UK) is investigated. Also in Refs. 22 and 23 this Kuramoto-like model was analyzed with respect to its application for power grids. These studies motivated further investigations of this model.[24–27]

Recently an extension of the model was proposed,[28] which not only includes the phase angles but also the voltage amplitudes. In a subsequent study, in particular the influence of non-Gaussian and intermittent statistics of the fluctuations of the power transfer was considered.[29]

[a)] Electronic mail: yannick.feld@uni-oldenburg.de; www.yfeld.de
[b)] Electronic mail: a.hartmann@uni-oldenburg.de; www.compphys.uni-oldenburg.de/en/

Previous studies on stability of power grids mainly considered either very small networks, like two coupled oscillators, or the analysis of medium-scale grids inspired by existing real-word transmission grids. If one wants to go beyond existing, engineering-like knowledge of how to construct very stable networks, a feasible approach could be to generate many random networks, evaluate the corresponding stabilities and try to identify the properties of the most (and least) stable ones. This could lead to design principles of which properties to seek and which to avoid. One basic finding in a previous study[25] was that "dead ends", i.e. nodes connected just to one other node (a *leaf* in graph theoretical language) should be avoided. In this study, 1000 randomly generated networks from the Erdős-Rény ensemble[30] were considered and each time the reaction of the network to node disturbances studied. Nevertheless, by sampling networks in this way, only *typical* networks with respect to the original ensemble will be generated. To understand better the origins or conditions of stability (or instability), one would rather like to sample extremely stable or unstable networks. For this reason recently large-deviation approaches[31,32] have been applied to study the distribution of the $N-1$ resilience for general transport networks[15] and for power-flow models.[17] This allowed the authors to reach extremely stable grids which by chance occur only with very small probabilities like 10^{-100}. By measuring other quantities of these networks, it was found out that often increasing the connectivity enhances stability, but this is a rather trivial effect (and costly in practice). Furthermore it was found[15,17] that networks exhibiting a small diameter[33] foster the stability of the grids. The large-deviation study of Ref. 17 also showed that on average a power-sign ratio smaller than 0.5 should be avoided for the creation of stable grids. Note that for the Kuramoto model a large sign ratio correlates with high synchronicity of the oscillators.[34,35]

To the knowledge of the authors, such a large-deviation study has not been performed for a dynamic power grid model. Thus, it is the purpose of the present work to investigate a dynamic stability of the Kuramoto-like model in a similar fashion.

To classify the stability of a synchronous (fixed) point of a power grid, we use *basin stability*.[25,36] It goes beyond nonlinear stability in the following way: A stable system is perturbed several times and it is measured how often the system returns to the stable point. Thus, the volume of the basin of attraction of the fixed point is estimated. Basin stability was studied in recent years several times[25,27,36–38] including the application to power grids.

We present the results of our study of the basin stability of the model by Filatrella et al.[19] for the ensemble of Erdős-Rényi (ER)[30] and small-world (SW)[39] networks. We investigated the probability distribution of the basin stability as well as correlations between stability and other properties of power grids or networks in general. We applied a large-deviation approach, in particular the $1/t$-algorithm,[40] which is an extension to the original Wang-Landau algorithm,[41] and subsequently entropic sampling.[42] In this way we were not only able to investigate the tails of the distribution, e.g., the probabilities of occurrence of particular stable grids, but also the properties of these grids by measuring the mentioned correlations to other quantities like number of leafs, network diameter or static stability measures.

The paper is organized as follows. Next, we present the details of the Kuromato-like model and the definitions of the network ensembles. In the third section, we explain the algorithms we have used and the quantities we have measured. In Sec. IV we present our results, followed by a summary and an outlook.

II. MODEL

A. Kuramoto-like model

The Kuramoto-like model, as derived by Filatrella et al.,[19] describes a set of N coupled oscillators i with phase $\theta_i(t)$. Their dynamic is defined by a system of coupled differential equations:

$$\ddot{\theta}_i = W_i - \alpha\dot{\theta}_i + K\sum_{j\neq i} \mathrm{A}_{ji}\sin(\theta_j - \theta_i) \qquad (1)$$

All parameters correspond to the renormalized parameter of the original work.[19] That means a phase velocity of $\dot{\theta}_i = 0$ corresponds to a node i, which is synchronized with the grid frequency of, e.g., 50Hz. K is the (global) coupling, α the (global) dampening and W_i is the power source (input/output) of oscillator i. A negative or positive power source corresponds to a consumer or generator respectively. The connectivity of the network is represented in the adjacency matrix $\mathbf{A}$ as

$$\mathrm{A}_{ij} = \begin{cases} 1 & \text{if } i,j \text{ connected} \\ 0 & \text{otherwise} \end{cases}. \qquad (2)$$

Note that the *degree* k_i of a node i is given by $k_i = \sum_j \mathrm{A}_{ij}$. Hence, within our model, an instance of an *energy grid* G is given by its underlying network, as defined by $\mathbf{A}$ and the distribution of power sources $\{W_i\}$.

For the purpose of this paper we used a binary distribution of the power sources, i.e.,

$$W_i \in \{-1, 1\} \qquad \text{and} \qquad \sum_i W_i = 0. \qquad (3)$$

That means, every generator is equal as is every consumer. Also there are as many generators as there are consumers. This ensures an overall power balance. The values of the other parameters are stated in Sec. IV A 1 and Sec. IV B 1.

B. Network ensembles

We investigated two ensembles, Erdős-Rényi[30] networks and small-world networks.[39,43,44]

Erdős-Rényi networks are constructed as follows. First generate N nodes with labels i.

Now, for each possible pair of nodes use an independent random number such that with probability

$$p = \frac{c}{N-1} \tag{4}$$

an edge is create between this pair, where c is the parameter determining the mean degree.

Our implementation of *small-world* networks consists of N nodes $i = 0, \ldots, N-1$, initially arranged in a ring. All nodes i are connected by edges $(i, i+1)$ and $(i, i+2)$ to their next and second-next neighbors (where nodes N and $N+1$ are identified with nodes 0 and 1). Next some edges are made "long-range", i.e., each edge (i, j) $j \in \{i+1, i+2\}$ is, with probability p, rewired as (i, j') with a randomly selected node $j' \neq i$. Here we used $p = 0.1$.

For any network type, depth first search is used to verify whether the constructed network is *connected*, i.e., there exists a path of edges between any pair of nodes. If not, the created network does not represent a valid energy network, so the whole network is discarded and the aforementioned construction process is restarted until a connected network is created. Finally, to complete a grid realization, for all nodes the corresponding values of W_i are drawn according to Eq. (3).

III. METHODS

Next, we present the approach we used to measure the dynamical stability of a given network using the basin stability. A natural approach to sample many networks, to explore the distribution of the stability, is simple sampling, which we explain in Sec. III B. To obtain the probability distribution down to very small probabilities, we use a Markov-chain based Monte Carlo approach, which we detail in Sec. III C to Sec. III E. Finally, we define the additional quantities we use to characterize the networks.

A. Basin stability

The basin stability was introduced by Menck et al.[36] as a simple however nonlinear way to characterize the stability of a desirable state against small or large perturbations. For any given grid G which is in a fixed point, stability here means the likelihood of returning to this fixed point after a perturbation. Therefore grids which are stable in this sense are resilient against fluctuations of the oscillators or of the environment.

The basic idea is to estimate the volume of the basin of attraction and use the relative size of this volume to quantify the stability of the current stable state. The stability measure turned out to be well suited for power grids modeled by the Kuramoto-like model.[25]

Basin stability can be implemented in different ways, e.g., one can perturb single or multiple nodes. Multiple-node (m-node) basin stability, as proposed by Mitra et al.,[37] is particularly suited to measure the stability of a grid as whole. Calculating the m-node basin stability ($m \geq 1$) works as follows:

Let the grid G be in its fixed point at some time t_0: $\theta_i(t_0) = \theta_i^{\text{fix}}$ for all nodes i. Note that Eq. (1) depends only on differences of phase angles, thus any global shift of the angles has no influence. In practice we normalize all angles by subtracting θ_0. We only consider those fixed points which are at least stable in the sense of a linear stability analysis (see Sec. III E). Now draw L random sets B_j each consisting of m distinct nodes. For each drawn set B_j perturb the nodes $i' \in B_j$ in the set by uniformly drawing random initial conditions $\theta_{i'} \in [-\pi, \pi]$ for all these nodes. Let the system continue its evolution according to Eq. (1) and determine whether the run returns to the initial fixed point. This is repeated U times for each set. F_j is the number of runs returning to the initial fixed point for set B_j. Then, the stability $S_m(G)$ of the grid G, is the set-averaged fraction of runs returning to the initial fixed point given by

$$S_m \equiv S_{L,m}(G) = \frac{1}{L} \sum_{j=1}^{L} \frac{F_j}{U} \,. \tag{5}$$

Note that we will omit L and G whenever the meaning is clear. For the purpose of this study we chose $U = 1$ runs per set, L different sets each exhibiting m nodes. Note that S_m can only assume $L+1$ different values due to the chosen parameters.

To determine whether an evolution is returning to the initial fixed point, a Runge-Kutta of 5th order with time step $\Delta t = 0.07$ is used to integrate the system for t_f time units (see Sec. III E). We consider the phase angle θ_i of a grid G to be returned if it deviates finally less than a threshold value θ_{th} from its fixed point $\theta_i^{\text{fix}} \equiv \theta_i^{\text{fix}}(G)$:

$$\Delta\theta_i(t) := \theta_i^{\text{fix}} - \theta_i(t) \tag{6}$$

$$\begin{aligned} &\text{if } |\Delta\theta_i(t_f)| < \theta_{\text{th}} \quad \forall i \rightarrow \text{stable} \\ &\text{otherwise} \qquad\qquad\quad \rightarrow \text{unstable} \end{aligned} \tag{7}$$

A run is counted as stable if condition Eq. (7) holds for *all* nodes i. In this paper we use $\theta_{\text{th}} = 0.05$.

In Fig. 1 an example for such a run is shown. This run is counted as unstable, since Eq. (7) does not hold for all i.

B. Simple sampling

To measure the probability density function (pdf) of the stability S with simple sampling, one has to create a grid for each sample independently. Then one can create a histogram $H(S)$ counting the occurrences of each stability. Let there be 10^k samples. Then the probability is

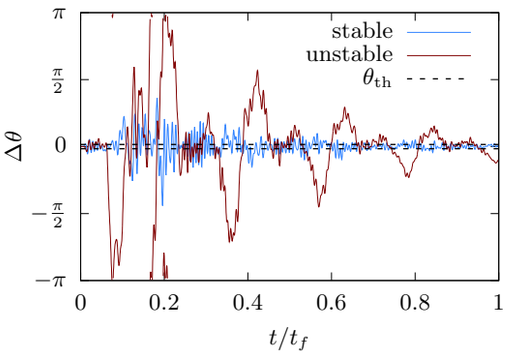

Figure 1. Example phase dynamics for a stable (light blue) and an unstable (dark red) oscillator of a run. The dashed lines indicate the magnitude of the threshold.

estimated as

$$p(S) \approx H(S) \cdot 10^{-k} \,. \tag{8}$$

That means, to resolve a probability of 10^{-k} one has to have at least 10^k samples.

C. Large-deviation Sampling

If one is interested in obtaining a probability distribution over a large range of the support, down to very small probabilities, specific large-deviation algorithms can be applied.[32] First application of such algorithms date back to the 1950 under the name of variance-reduction techniques.[45] In physics, these techniques became better known, e.g., via the application of transition-path sampling[46] to study dynamics of molecules. In statistical physics the approach was used, among other applications, to investigate the statistics of sequence alignment,[47] the properties of random networks[48–51] or of non-equilibrium processes.[52–54]

The approach we applied here is based on the Wang-Landau (WL) algorithm.[41] The basic idea of the algorithm is as follows: Let $g(S)$ be a non-normalized estimate for the density of states for the stabilities S, which is determined by the ensemble of random grids G and their corresponding stabilities $S = S(G)$. Clearly, $g(S)$ is the target quantity and not known beforehand. Thus, the WL algorithm starts with an unbiased guess $g(S) = 1$ $\forall S$ and the basic aim is to determine the correct density $g(S)$. This works by performing a random walk in grid space, i.e., creating a *Markov chain* of states, which are realizations of grids here. As usual each visited state is only dependent on the previous state and transition rates between states.

Let G_n be the grid at step n of the Markov chain and $S_n = S(G_n)$ its basin stability Eq. (5). Now, a trial grid G' is generated from G_n, by changing edges and generators slightly, for details see Sec. III D. This trial grid exhibits a stability $S' = S(G')$. WL tells us to accept the trial grid, i.e., use $G_{n+1} = G'$ with a Metropolis-Hastings probability

$$p_{\rm acc} = \min\left(\frac{g(S_n)}{g(S')}, 1\right) \,. \tag{9}$$

If the trial grid is not accepted, the current grid is kept, i.e., $G_{n+1} = G_n$.

The estimate $g(S)$ is updated at $S = S(G_{n+1})$ with a multiplicative factor $f > 1$, i.e., $g(S(G_{n+1})) \to f \cdot g(S(G_{n+1}))$, each step during the simulation, which is intended to converge to the sought-after pdf. At the beginning f is rather large, like $f = e \approx 2.71$ and reduced towards 1 during the simulation.

The original algorithm has problems with the saturation of the final error as pointed out originally by Ref. 55 (see also Refs. 40, 56, and 57). To circumvent the problem, Belardinelli and Pereyra introduced an algorithm,[40] which is based on Wang-Landau but f is updated differently, mainly $\log(f) \propto 1/n$, where n is again the Markov time. It was shown, that the this algorithm does not suffer from error saturation.[56]

Since the WL algorithm and its variants suffer from the lack of detailed balance, we perform entropic sampling[42] afterwards. This means, we start with the estimate $g(S)$ as computed by WL. We again perform a Markov chain of states, i.e., grids, according to the Metropolis-Hastings probability Eq. (9). The only difference to WL is that the density estimate g is not updated any more.

Instead, a histogram of visited stabilites $H(S)$ is maintained. As the last step of the simulation, the probability density $P(S)$ is calculated. First, from a non-normalized combination of $g(S)$ and $H(S)$:

$$\widetilde{P}(S) = \begin{cases} g(S) & \text{if } H(S) = 0 \\ g(S) \cdot H(S) & \text{otherwise} \end{cases} \tag{10}$$

and finally normalizing $P(S) = \widetilde{P}(S) / \int_{\tilde{S}} \widetilde{P}(\tilde{S}) d\tilde{S}$. For our simulations, the entropic sampling used the same number of steps as the WL sampling. We also verified that the case $H(S) = 0$ did not occur.

To make the calculation of the probability density function over the whole stability regime more feasible, we split the stability range into multiple overlapping intervals.[58,59] For each interval we performed a WL plus an entropic sampling simulation. To obtain a full pdf, we finally merged the resulting pdfs, which can be done, since the pdfs of the overlapping regions have to match, at least within statistical fluctuations.[41,47] This was also used as stopping criterion for the WL algorithm by terminating when the overlapping regions match sufficiently.

We chose to investigate a global stability measure because there are no special nodes, as all nodes are treated the same in the ensembles. If, however, one had an ensemble where nodes are distinguishable, for example if one would look at a specific grid topology and was interested in the influence of the placement or the output

W_i of the power sources, the described large-deviation techniques could also be applied to investigate a local stability measure instead.

D. Change move

The Markov chain simulation is build on a basic change move to generate trial grids allowing to perform the random walk in the ensemble of power grids. The change move we used works as follows.

For the Erdős-Rényi ensemble: Draw a pair i, j of nodes. Remove the edge $\{i, j\}$ connecting the drawn node pair if it exists. Create an edge between the nodes with probability p (see Sec. II B).

For the small-world ensemble: Draw an edge (i, j). With probability $1 - p$ the edge is reset to its original state in the ring. Otherwise it is rewired with a random node j', i.e. $(i, j) \to (i, j')$.

Repeat this τ times. This τ determines the *change size* in each step. Finally, draw another pair i, j and exchange the values $W_i \leftrightarrow W_j$.

If the resulting trial network is not connected the trial grid will be rejected immediately in the Markov Chain. Otherwise the trial grid is accepted with the probability depending on the basin stability of the two power grids (see Sec. III C Eq. (9)).

In order to achieve an efficient change step, the change size τ is not a fixed value, but will be chosen for each step randomly as explained below:

The basic idea is to gather statistics on how the empirical acceptance frequencies depend on the change size. Thus, two histograms are created, one $H_r(\tau)$ for counting rejected moves and $H_a(\tau)$ one for counting accepted moves. We assume that an empirical acceptance of 0.5 is good, but allow for change sizes exhibiting similar acceptance frequencies.

Initially, or when the value of f is changed, we start building new acceptance statistics. Then, we chose a maximum change size $\tau_{\max}$. Now, each possible change size $\tau \in \{1, \ldots, \tau_{\max}\}$ used during the WL simulations is tried $l = 50$ times, in random order. Technically we used a list of $l \cdot \tau_{\max}$ change sizes, from which one change size is taken randomly and used whenever a change move is performed. This is used to build up initial statistics $H_r(\tau)$ and $H_a(\tau)$.

Using these statistics, we obtain an empirical τ-depended acceptance rate $f_{\mathrm{acc}}(\tau) = \frac{H_a(\tau)}{H_a(\tau)+H_r(\tau)}$. Next, we construct a subset $M_\tau = \{\tau \mid 0.5 - \Delta f \leq f_{\mathrm{acc}}(\tau) \leq 0.5 + \Delta f\}$ of change sizes such that they exhibit empirical acceptance rates in a window of size $2\Delta f = 0.3$ around the desirable acceptance rate 0.5. If the set M_τ is too small, e.g., smaller than 7, we add iteratively those changes sizes which exhibit an acceptance rate closest to 0.5 until the set size 7 is reached. During the WL and entropic sampling simulations, unless the statistics are rebuild as explained above, we always draw the change size randomly and uniformly from the set M_τ. Anyway, the acceptance histograms $H_r(\tau)$ and $H_a(\tau)$ are updated during the remainder of the simulation and the set M_τ of change sizes is occasionally adapted.

Note that this adaptive approach is rather independent of the Monte Carlo algorithm used and of the problem investigated and might be useful for other types of Monte Carlo simulations.

E. Technicalities

For the Monte Carlo simulations we want to always get the same stability for the same network. We therefore fix the seeds of the random number generator for the perturbances to always draw the same L sets of nodes B_j (see Sec. III A) and to always get the same values θ_i $i \in B_j$ for the initial conditions. Note that the initial distance to the fixed point $\Delta\theta_i(0)$ of the nodes $i \in B_j$ varies, since the fixed point is dependent on the grid realization.

To find the fixed point of Eq. (1), we use a Newton-Raphson algorithm (modified version from Ref. 60). To check if a stable[61,62] fixed point was found, we then check if all eigenvalues are smaller than 0. If not, we try different starting points for Newton-Raphson. For example the solution of the linearized equations or by using a few Runge-Kutta steps. If no fixed point could be found using this method, the corresponding network was discarded, since the basin stability could not be calculated.

To integrate the equations, we use a Runge-Kutta[60,63–67] algorithm of fifth order with step size $\Delta t = 0.07$. At the end, one calculates the fraction of trajectories, which are sufficiently close to the fixed point after a fixed amount of time t_f.

F. Measurable quantities for correlation

Since we are interested in finding properties of extremely stable or unstable networks, we measure also other properties of the grids we encounter during the large-deviation simulations, i.e., each time we wrote S_m to a file, we also wrote the values for all other quantities. We are interested in those properties which correlate with the stability (or instability). They could also serve as design guidelines to create stable networks. Next we give short, where necessary also more detailed, definitions of the quantities we have investigated.

1. Diameter

For two nodes i, j which are connected in a network having N nodes and M edges, there exists at least one, possibly many, paths connecting them. The shortest among them, measured in terms of number of edges, is the *shortest path*, sometimes called *geodesic path*.[33] It can be obtained conveniently by breadth-first search, which can be done for a connected graph[68] in time $\mathcal{O}(M)$. For

a given network, the longest geodesic path among all pairs i, j is called the *diameter* d. Correspondingly, it can be obtained by repeated breadth-first search, i.e., in $\mathcal{O}(NM)$.

2. Flow backup capacity

The *backup capacity* P_F is a measurable quantity that was investigated in an earlier work on the stability of networks with a power-flow model.[17] The redundant capacity K_{ab}^{red} defined later on by Witthaut et al.[24] is related to the backup capacity.

To define the backup capacity we transform Eq. (1) to the power-flow model, which describes the stationary state. This is achieved by setting $\dot{\theta}_i = \ddot{\theta}_i = 0$, with the argument of being interested only in the fixed points of Eq. (1). Together with a linearization of the sine, that leads to

$$W_i = -K \sum_j \mathrm{A}_{ij} \left(\theta_j - \theta_i\right) . \tag{11}$$

Since only the phase differences are of interest, one can choose one phase $\theta_0 = 0$. The linearized equations can be solved for θ_i by standard Gaussian elimination.[69]

The power flow K_{ij}^{flow} between connected nodes can be calculated as

$$K_{ij}^{\mathrm{flow}} = \left| K \mathrm{A}_{ij} \sin\left(\theta_j - \theta_i\right) \right| . \tag{12}$$

To simulate a failure, the transmission line with highest load K_{ij}^{flow} is removed and the resulting new power flows $\widetilde{K}_{ij}^{\mathrm{flow}}$ are calculated.

The backup capacity is defined as a $N-1$ stability measure, i.e., the grid should provide enough additional capacity to take care of the increased flow

$$P_F = \max_{i,j} \left(\widetilde{K}_{ij}^{\mathrm{flow}} - K_{ij}^{\mathrm{flow}} \right) . \tag{13}$$

If the removal of the line with highest load disconnected the network $P_F = \infty$.

3. Power-sign ratio

The *power-sign ratio* $\upsilon_{\pm}$ is a measurable quantity that was investigated in an earlier work on the stability of networks with a power-flow model.[17] It is defined as the fraction of edges that connect W_i with opposite signs and the total number of edges in the network.

4. Universal order parameter

The *universal order parameter*[70] r_{uni} describes the phase coherence of the oscillators,

$$r_{\mathrm{uni}} = \frac{1}{\sum_i k_i} \sum_{i,j} \mathrm{A}_{ij} \left\langle \cos\left(\theta_i - \theta_j\right) \right\rangle_t \tag{14}$$

where $\langle \ldots \rangle_t$ denotes a suitable time average. We are interested in the fixed points of the grid, where $\ddot{\theta}_i = \dot{\theta}_i = 0$. We therefore simplify the equation

$$r_{\mathrm{uni}} = \frac{1}{\sum_i k_i} \sum_{i,j} \mathrm{A}_{ij} \cos\left(\theta_i^{\mathrm{fix}} - \theta_j^{\mathrm{fix}}\right) . \tag{15}$$

This order parameter is closely related to the complex order parameter $r(t)\exp(\mathrm{i}\Psi(t)) = N^{-1}\sum_j \exp(\mathrm{i}\theta_j)$ for the Kuramoto model.[20,71,72]

5. Biconnected component

The *biconnected component* (*bicomponent*) of a network is defined as the maximal subset of nodes, where every node can be reached by at least two node-independent paths from each other node of the subset.[33] Large-deviation properties of the biconnected component for the ensemble of Erdős-Rényi random graphs were studied in Ref. 51 We investigate the size N_{bi}, measured in terms of the number of nodes, of the largest biconnected component.

"Algorithm 447" is an efficient[73] way to calculate the biconnected component and thus used in this study.

6. Transitivity and clustering coefficient

The *transitivity* C_T is a standard property measured for graphs and describes the relative abundance of *triangles*[74] (small *loops*) in a graph. It is defined as the number of closed paths of length three divided by the total number of paths of length two.[33]

The transitivity was proposed by Newman, Watts and Strogatz[75] in 2002, though it seems they thought it was just an alternative description for the *average local clustering coefficient* C_l that was defined by Watts and Strogatz[39] in 1998. However C_T and C_l are different quantities,[76,77] although they are very similar.

7. Two core

The *two core* K_2 of a graph, see e.g., Ref. 78, is the subset of nodes which is obtained by iteratively removing all nodes i which have a degree k_i smaller than two. Note that through removal of a node another node will decrease its degree such that it may become eligible for removal as well. Hence, the iteration stops if all nodes have degree two or more.

8. Degree count

The number of nodes N_k with degree k can easily be obtained by

$$N_k = \sum_i \delta_{k_i,k} \,. \tag{16}$$

IV. RESULTS

Next, we present the results of our simulations. First, we show the results of an Erdős-Rényi ensemble and second for a small world ensemble.

A. Erdős-Rényi

The Erdős-Rényi model is the most simple model for random networks because it makes no assumption about the topology except the average number of neighbors. Therefore, it serves as a useful null model for any investigation of networks.

1. Simulation details

For the Erdős-Rényi grids we chose $K = 8$, $N = 50$, and $c = 2.7$ in Eq. (4) restricted to the subset of connected networks, i.e., which exhibit just one connected component. Furthermore, we chose $\alpha = 0.035$ and $W_i = \pm 1$. These are similar parameters to the ones used in Ref. 25, though they used $N = 100$ and $\alpha = 0.1$ instead. We have chosen to study a smaller value of the dampening α since for $\alpha = 0.1$ most networks are stable and thus the results less interesting.

For the calculation of the basin stability we used $L = 200$ different sets each exhibiting $m = 5$ nodes. Since this means, that the basin stability S_m can only assume 201 values in this particular case, we will use these values to define the bins needed for the large-deviation simulations. For the Runge-Kutta algorithm we used a duration of $t_f = 180$ time units (and the Δt value mentioned in Sec. III A.

As mentioned in Sec. III E, a given (trial) grid encountered during simple sampling, the Wang-Landau simulation or the entropic sampling was discarded if no fixed point of Eq. (1) could be found. The frequency of not finding the fixed point were $2.7 \cdot 10^{-6}$ during the simple sampling, $3.5 \cdot 10^{-5}$ during WL and $2.5 \cdot 10^{-5}$ during entropic sampling.

For WL and entropic sampling four intervals covering 80% of the support, i.e., $S_m \in [0, 0.8]$, were used. Each entropic sampling interval visited the left and right border alternatingly for at least 12 times, which means that the simulation is well "equilibrated".

2. Probability density function

The pdf for the basin stability of the ER grids is shown in Fig. 2. By using the large-deviation approach, we were able to obtain the pdf over a large range of its support, extending over eight decades in probability. For comparison, we also show the simple sampling results of $3.75 \cdot 10^5$ independently generated grids. For the simple sampling to achieve a good statistics, a bin had to be visited at least 100 times to be shown in the plot. This means, by applying the large-deviation approach, we were able to observe $P(S_5)$ with good statistical quality over five more decades in probability as compared to simple sampling. For larger values of N, this advantage of the large-deviation algorithm would likely be even higher. Note that we evaluated about $3.4 \cdot 10^6$ grids during the large-deviation simulations, i.e., roughly one decode as many grids as we evaluated for the simple sampling approach. This means the computational advantage corresponds to five minus one equals four decades.

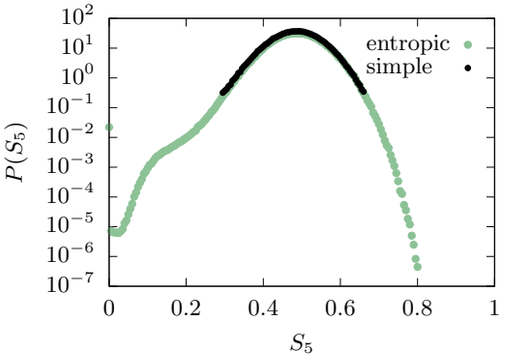

Figure 2. $P(S_5)$ for ER grids measured with entropic sampling and, for comparison, simple sampling.

As one can see, typical graphs exhibit a stability of about $S_5 \approx 0.5$ for these parameters. The most unlikely grids are the most stable ones. Note that grids which exhibit basin stability $S_5 = 0$ appear with a probability of $P(0) \approx 10^{-2}$ far more often than grids which rareley but sometimes find back to the fixed point.

3. Correlations

As mentioned above, we are interested in finding which grid properties are in particular determining the stability of the grid. Thus, we measured various quantities Q during our sampling.

To analyze the results, we display two-dimensional "heatmaps" Q versus S_m, binned according to the values of S_m, with a color code which displays the probability $p(Q|S_m)$ to find a certain value of Q conditioned to a value of S_m. Note that $p(Q|S_5)$ is normalized, i.e., $\int_Q p(Q|S_5) dQ = 1$. The respective figure also shows the

average $\overline{Q}(S_5) := \int_Q Q\ p(Q|S_5)dQ$ for each bin.

For the analysis we always used the data set we obtained from entropic sampling. Furthermore, in addition to the heatmaps we always computed the linear correlation coefficient $R_Q = R_{Q,S_m}$ between Q and S_m such that each bin contributes the same number of points as well as the correlation $R_{\overline{Q}} = R_{\overline{Q},S_m}$ between the average $\overline{Q}$ and S_m (which neglects fluctuations and leads to higher values).

In Fig. 3 we show the heatmap for the number N_1 of nodes with degree 1, also called *leafs*. For values $S_m > 0.3$ a clear correspondence between a strong stability and a small number of leafs is visible, while for less stable grids no clear influence could be observed. This is reflected by the linear correlation coefficients $R_{N_1} = -0.8$ and $R_{\overline{N_1}} = -0.94$. Thus, the more stable the power grid is, the less leafs its network exhibits, although the least stable grids cannot be explained by N_1 alone. The general result supports the findings of Refs. 25 and 38, who concluded from a simple-sampling simulation, which is the range with the strongest correlation for our results as well, that tree-shaped structures and dead-ends should be avoided for the creation of stable grids.

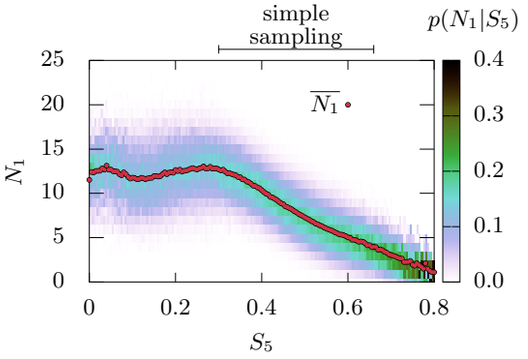

Figure 3. Heatmap indicating the probability $p(N_1|S_5)$ for a power grid to exhibit N_1 nodes with degree 1, i.e., leafs, conditioned to a stability S_5. The average $\overline{N_1}$ as a function of S_5 is also shown. The range easily reachable with simple sampling is indicated by the bar above the figure.

These rules of thumb of Refs. 25 and 38. are even more supported by the result for the size N_{bi} of the biggest biconnected component, i.e., a structure of the graph which is not tree like. The heatmap is shown in Fig. 4. Here the correspondence between stability and component size seems to be even stronger than for the case of N_1. For very small stabilities of $S_5 < 0.04$ a smaller N_{bi} seems to correlate with a more stable grid, though this might be a *finite-size effect*.[79] Generally speaking the more stable the grid is, the larger is its largest biconnected component. Thus not only the leafs, but in particular the nodes which are located on single paths to the leafs are a major reason for less-stable grids. We measured linear correlation coefficients of $R_{N_{\mathrm{bi}}} = 0.85$ and $R_{\overline{N_{\mathrm{bi}}}} = 0.98$.

We found a very similar pattern (not shown) for the

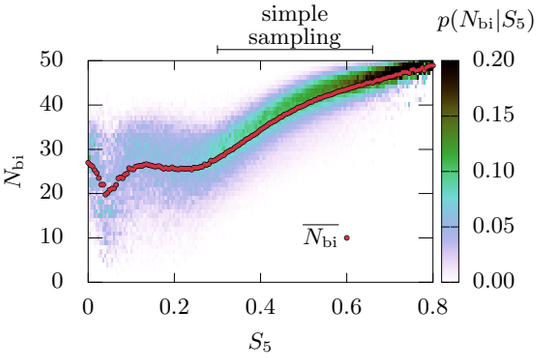

Figure 4. Heatmap indicating the probability $p(N_{\mathrm{bi}}|S_5)$ for the largest biconnected component N_{bi} of a power grid conditioned to a value S_5. For reference the average $\overline{N_{\mathrm{bi}}}$ as a function of S_5 is also shown. The range easily reachable with simple sampling is indicated above.

two core, which is for ER random graphs very similar to the biconnected component.[51] Here we measured slightly smaller linear correlation coefficients of $R_{K_2} = 0.83$ and $R_{\overline{K_2}} = 0.96$.

In Fig. 5 we show the heatmap for the diameter d, for which in previous works[15,17] of static grid models a notable correlation was found. Here we also see that smaller diameters lead to more stable grids. For small stabilities, however, there seems to be a reversal of this correlation. This might be a finite-size effect or it could be an occurrence of Braess's paradox,[80] i.e., adding an edge might not decrease but instead increase the load on other edges, which in turn can destabilize the system.[81] We measured linear correlation coefficients of $R_d = -0.83$ and $R_{\overline{d}} = -0.97$.

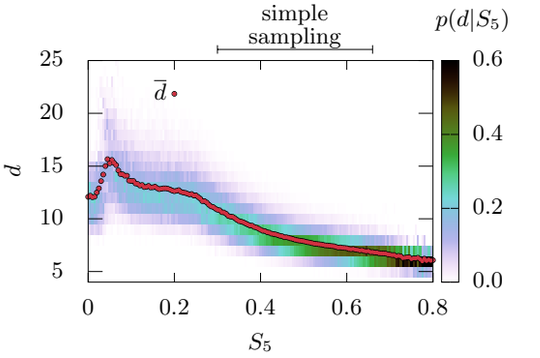

Figure 5. Heatmap indicating the conditional probability $p(d|S_5)$ for a grid with stability S_5 to exhibit the diameter d. For reference the average $\overline{d}$ as a function of S_5 is also shown. The range easily reachable with simple sampling is indicated above.

We also measured the stability measure used in Ref. 17, the flow backup capacity P_F and show the resulting heatmap in Fig. 6. We were able to observe a good cor-

relation for $S_5 > 0.4$. Here, especially for $S_5 < 0.4$, it happened frequently that the investigated networks were connected, as required, but the line with the highest load was not part of the biconnected component, which means $P_F = \infty$. Thus, we had to exclude these grids from our statistics. Overall this effected about half of the grids encountered during the entropic sampling simulation, which resulted in very bad statistics for $S_5 < 0.4$ for this correlation. We measured the linear correlation coefficients of $R_{P_F} = -0.83$ and $R_{\overline{P_F}} = -0.94$, though they are effected by the bad statistics. Nonetheless the correlation with the basin stability indicates, that a low backup capacity is preferable for the creation of stable grids.

So far we have used linear correlation coefficient to quantify the dependence between some parameters and the basin stability. Nevertheless, as in particular visible for the flow backup capacity, the dependence sometimes deviates considerably from the linear behavior. For this reason we assume a more complicated dependency here. We used a heuristic approach to fit a curve through the average $\overline{P_F}$. It allows for a sigmoidal shape as well as non-horizontal behavior in the left part (this is in particular motivated by the result for the small-world grids as shown in the next section). We therefore used a hyperbolic tangent multiplied with a function approaching 1 for large S_m and arrived at the function

$$h(S_m) = \beta_1 \left(\beta_2 + \tanh(-\beta_3(S_m + \beta_4))\right)\left(1 + e^{-S_m \beta_5}\right). \tag{17}$$

The obtained fit parameters are $\beta_1 = 1.31(8)$, $\beta_2 = 1.4(1)$, $\beta_3 = 5.9(5)$, $\beta_4 = -0.25(2)$ and $\beta_5 = 0.4(7)$. Visually the fit works well, however the error for β_5 is significantly large, probably due to bad statistics for small values of S_5.

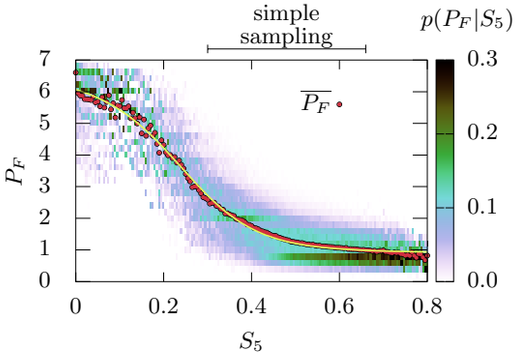

Figure 6. Heatmap indicating the conditional probability $p(P_F|S_5)$ for a grid with stability S_5 to exhibit the backup capacity P_F. For reference the average $\overline{P_F}$ as a function of S_5 is also shown. The yellow line was fitted to the average using Eq. (17). The range easily reachable with simple sampling is indicated above.

The measurement of the power-sign ratio $\upsilon_\pm$ (not shown here), which in a past work[17] exhibited a strong correlation to the static stability, resulted in linear correlation coefficients of $R_{\upsilon_\pm} = 0.41$ and $R_{\overline{\upsilon_\pm}} = 0.90$. A larger basin stability is correlated to a larger power-sign ratio, but it seems like, on average, a power-sign ratio of about $\upsilon_\pm \approx 0.5$ is enough for the creation of very stable grids and there seems no benefit in having a larger $\upsilon_\pm$, which is similar to the results[17] for the static stability measure. Overall the correlation is visible, but not as strong as in the study of the static grids.

We also looked at the transitivity C_T and the local clustering coefficient C_l (no heatmaps shown here). In general we observed strong fluctuations, correspondingly, we found rather small linear correlation coefficients of $R_{C_T} = 0.068$ and $R_{C_l} = 0.22$. Thus, the transitivity seems to be less correlated with the basin stability than the local clustering coefficient. The same can be seen for the correlation coefficients of the averages where we obtained $R_{\overline{C_T}} = 0.72$ and $R_{\overline{C_l}} = 0.94$. Overall small triangles do not seem to matter much for the stability of grids from the Erdős-Rényi ensemble we investigated.

Finally, in Fig. 7 we show the heatmap for the universal order parameter r_{uni}. Note that a small, but for the average significant, amount of grids, e.g., 1.1% for $S_5 = 0.1$, exhibits vastly smaller values $r_{\text{uni}} \leq 0.6$. These values are not visible in the chosen range of the heatmap.

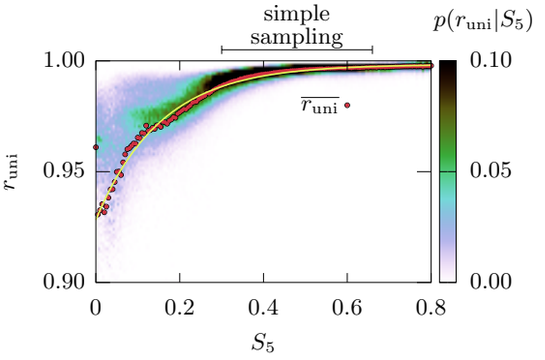

Figure 7. Heatmap indicating the probability $p(r_{\text{uni}}|S_5)$. For reference the average $\overline{r_{\text{uni}}}$ as a function of S_5 is also shown. The yellow line was fitted to the average using Eq. (18). The range easily reachable with simple sampling is indicated above.

The parameter r_{uni} does not change much for $S_5 > 0.4$, though the correlation is clearly visible for $S_5 < 0.4$. We measured linear correlation coefficients of $R_{r_{\text{uni}}} = 0.41$ and $R_{\overline{r_{\text{uni}}}} = 0.85$. Anyway, over the measured range of values of S_5, the result for r_{uni} is rather large, indicating the the grids in this ensemble are well synchronized and S_5 indeed is a qualitatively different measure of the behavior, beyond the steady-state operation (which is addressed by r_{uni}). Nevertheless, the fact that the universal order parameter is in particular close to one for $S_m > 0.4$, indicates that high phase coherence is indeed necessary for the most stable grids regarding the basin of attraction.

Looking at $\overline{r_{\text{uni}}}$ in Fig. 7 it seems like, excluding $S_5 = 0$, one could describe the behavior of the average with a

function like

$$f(S_m) = \kappa_1 - \kappa_2 e^{-S_m \kappa_3} \,. \tag{18}$$

We therefore used Eq. (18) to fit a curve through the average and show the results in the heatmap. The fit parameter were $\kappa_1 = 0.9984(2)$, $\kappa_2 = 0.0702(6)$ and $\kappa_3 = 6.5(1)$.

B. Small-world

Secondly a widely studied model of networks is considered here, the *small-world* (SW) ensemble.[39,43,44] This ensemble was found to represent the U.S. power grid well.[12,39,43] Due to the construction process of the small-world networks (see Sec. II B), every node i has at least degree $k = 2$. This means, that the examined ensemble does not allow for dead ends or tree shaped structures, hence, as we have seen in the previous section and as it was shown in previous works[25,38] a major source of dynamic instability is avoided. We are therefore able to observe better the correlation between basin stability and other measurable quantities independent from the impact of dead ends or trees.

1. Simulation details

For the small-world grids we chose the same parameter as used for the ER ensemble, i.e., $K = 8$, $N = 50$, $\alpha = 0.035$ and $W_i = \pm 1$. For the calculation of the basin stability we used $L = 200$ different sets each exhibiting $m = 5$ nodes. For Runge-Kutta we used a duration of $t_f = 180$ time units (and the Δt value mentioned in Sec. III A).

As for the ER networks, a given grid was discarded if no fixed point could be found. The fractions of not finding the fixed point were $2.3 \cdot 10^{-5}$ during the simple sampling, $3.9 \cdot 10^{-5}$ during WL and $1.6 \cdot 10^{-5}$ during entropic sampling.

For WL and entropic sampling we performed the simulations for 8 intervals covering the range of $S_m \in [0, 0.81]$. Entropic sampling visited the left and right border alternatingly at least 10 times, which means that the simulation is well enough "equilibrated".

2. Probability density function

The measured pdf $P(S_m)$ of the basin stability for the small-world ensemble can be found in Fig. 8. For the simple sampling, which is included for comparison, we measured about $3 \cdot 10^5$ independent grids. To achieve good statistics every bin had to be visited at least 100 times to be used in the plot. This covers about 40% of the support, i.e., $S_m \in [0.4, 0.8]$. By using the large-deviation approach, we are able to double this range, allowing us to study very stable and very unstable grids, which are otherwise out of reach. Note that during the large-deviation sampling we evaluated about $3.2 \cdot 10^6$ grids, i.e., roughly ten times as much as during our simple sampling. Since the large-deviation sampling allowed us to study $P(S_m)$ over five more decades in probability, this results in a computaional advantage of four decades.

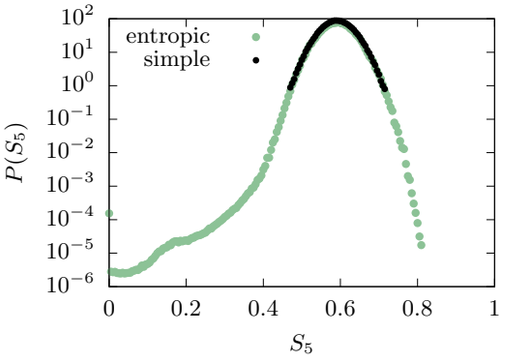

Figure 8. $P(S_5)$ for small-world graphs with $N = 50$ nodes and 4 neighbors on average, measured with entropic sampling and, for comparison, simple sampling.

In comparison to the result for ER graphs shown in Fig. 2, the most probable grids exhibit a slightly larger stability. This was expected, because networks from the small-world ensemble do not exhibit leafs and have a higher number of neighbors (4) on average compared to the ER case. The correlations between the basin stability S_m and other measurable quantities Q are also different here to some extend.

3. Correlations

Trivially, since the small-world networks exhibit only nodes with degree at least two, it does not make (much) sense to study the correlation of S_m with the number of degree-one nodes, the size of the two-core or the size of the largest biconnected component.

Thus, we proceed with the diameter d. In Fig. 9 we show the heatmap $p(d|S_m)$ for the SW ensemble. As previously, the grids exhibiting the largest stability come with the smallest diameter. We measured linear correlation coefficients of $R_d = -0.6$ and $R_{\overline{d}} = -0.83$. Compared to the correlations observed in Fig. 5 this is not only significantly less, but we also observe a partial reversal of the behavior. Although for values $S_m > 0.36$ we observe that a smaller diameter correlates with a more stable power grid, for stabilites $S_m < 0.36$ the reverse seems to be true, on a smaller scale. This might have to do with the fact that the SW ensemble does not exhibit leafs here and therefore a larger diameter does not lead to more leafs, which would have a high impact on the stability. Thus, here the influence of other grid properties on the stability come into play.

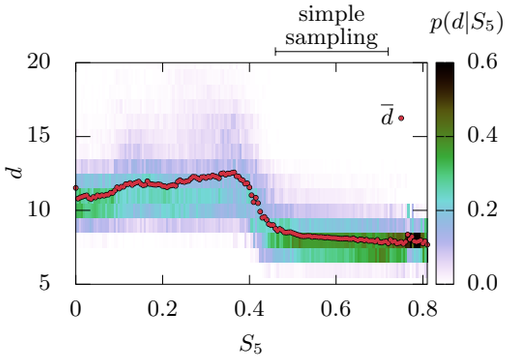

Figure 9. Heatmap indicating the probability $p(d|S_5)$ for a grid with stability S_5 to exhibit the Diameter d. For reference the average $\overline{d}$ as a function of S_5 is also shown. The range easily reachable with simple sampling is indicated above.

In Fig. 10 we show the heatmap for the universal order parameter r_{uni}. Note that here in the range $S_m < 0.4$ a small but significant fraction of grids exhibit rather small values $r_{\text{uni}} \leq 0.6$ (not visible in the plot with the chosen range). For this reason the average $\overline{r_{\text{uni}}}$ is here located slightly below the most probable values of the order parameter. The behavior is similar to the behavior seen in Fig. 7. We measured linear correlation coefficients of $R_{r_{\text{uni}}} = 0.27$ and $R_{\overline{r_{\text{uni}}}} = 0.95$. The dependency is monotonous and the grids exhibiting the smallest stabilities go along with the on average smallest values for r_{uni}. Thus, although the correlation, i.e., the influence of this order parameter on the stability, is in general weaker than the influence of the diameter, it is more important to explain the behavior of the very unstable grids exhibiting $S_m < 0.1$.

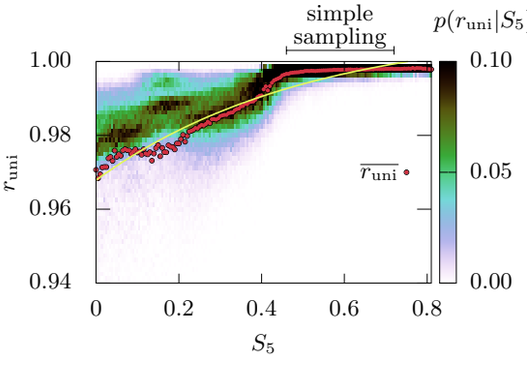

Figure 10. Heatmap indicating the probability $p(r_{\text{uni}}|S_5)$. For reference the average $\overline{r_{\text{uni}}}$ as a function of S_5 is also shown. The yellow line was fitted to the average using Eq. (18). The range easily reachable with simple sampling is indicated above.

Since we used Eq. (18) to fit a curve to the average $\overline{r_{\text{uni}}}$ for the ER ensemble, we used the same fit here. The fit parameter were $\kappa_1 = 1.009(2)$, $\kappa_2 = 0.041(3)$ and $\kappa_3 = 2.0(2)$. This time the fit does not work well, but at least captures somehow the linear dependency for small stability values followed by a decrease of slope.

Next, we compare the (dynamic) basin stability with the (static) $N-1$ stability criterion of the backup capacity. Since the SW ensemble exhibits usually biconnected graphs, the case $P_F = \infty$ is not as problematic as before and we can obtain the correlations with good statistics using the large-deviation approach everywhere. In Fig. 11 we show the heatmap for the backup capacity P_F. We measured linear correlation coefficients of $R_{P_F} = -0.9$ and $R_{\overline{P_F}} = -0.95$. We see a clear and strong correlation especially for the unstable grids. This is particularly interesting since the backup capacity was already studied with a large-deviation approach.[17] Evidently for the well connected SW ensemble static and dynamic stability go well along with each other.

Again we investigated the correspondence going beyond linear correlations by fitting to Eq. (17). The obtained fit parameter corresponding to Fig. 11 are $\beta_1 = 0.800(3)$, $\beta_2 = 1.62(1)$, $\beta_3 = 18.9(5)$, $\beta_4 = -0.4089(8)$ and $\beta_5 = 1.65(5)$.

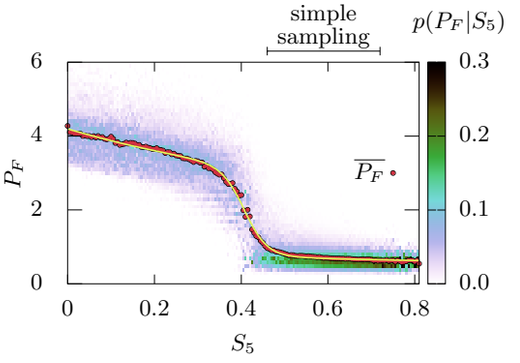

Figure 11. Heatmap indicating the probability $p(P_F|S_5)$ for a grid with stability S_5 to exhibit the backup capacity P_F. For reference the average of P_F as a function of S_5 is also shown. The yellow line was fitted to the average using Eq. (17). The range easily reachable with simple sampling is indicated above.

For the case of the static $N-1$ stability concerning the power flow a very strong correlation between the backup capacity P_F and the power-sign ratio $\upsilon_\pm$ was found.[17] Thus, we show here in Fig. 12 the heatmap for $\upsilon_\pm$. A very clear correspondence is visible. We measured linear correlation coefficients of $R_{\upsilon_\pm} = 0.71$ and $R_{\overline{\upsilon_\pm}} = 0.95$. Thus, as a rule of thump, attempting a power-sign ratio of $\upsilon_\pm \approx 0.5$ seems to be preferable for the construction of dynamically stable grids. In particular, as the results from range $S_m < 0.5$ show, which we obtained only through the large-deviation approach, low power-sign rations smaller than 0.5 should be avoided.

Finally, we tried to investigate whether the presence of small loops, i.e., triangles, has an influence. In Fig. 13 we show the heatmap for the transitivity C_T. A significant

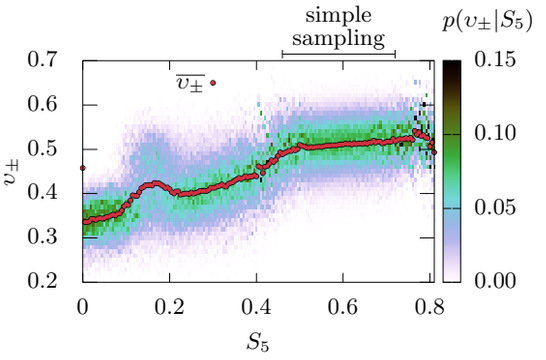

Figure 12. Heatmap for the probability $p(\upsilon_\pm|S_5)$ for a grid conditioned to the stability S_5 to exhibit the power-sign ratio $\upsilon_\pm$. For reference the average $\overline{\upsilon_\pm}$ as a function of S_5 is also shown. The range easily reachable with simple sampling is indicated above.

negative correlation is visible. We measured linear correlation coefficients of $R_{C_T} = -0.60$ and $R_{\overline{C_T}} = -0.92$. Interestingly we measured the same correlation coefficients for the clustering coefficient C_l (no heatmap shown), i.e., $R_{C_l} = -0.60$ and $R_{\overline{C_l}} = -0.92$.

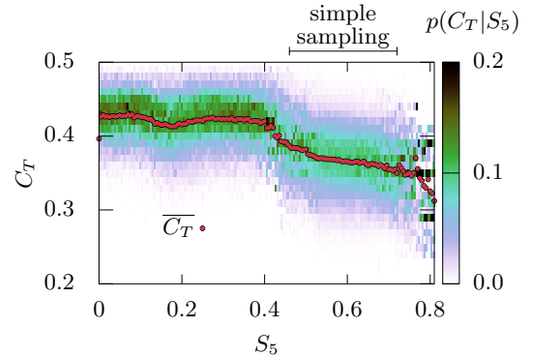

Figure 13. Heatmap showing the probability $p(C_T|S_5)$ to exhibit the transitivity C_T for a grid conditioned to the stability S_5. For reference the average $\overline{C_T}$ as a function of S_5 is also shown. The range easily reachable with simple sampling is indicated above.

The correlation is surprising, considering we noticed no noteworthy correlation for the Erdős-Rényi ensemble. It should be noted that the underlying regular ring network of the SW ensemble exhibits many triangles. Thus, the rerouting of links to create long-range connections, which leads to smaller diameter and thus more stable grids, will inevitably reduce the fraction of triangles. Thus, it appears likely to us, that the correlation we observe here is rather an indirect result of the appearance of many long-range links for grids exhibiting a high basin stability.

V. SUMMARY

We investigated the basin stability S_m, which measures the dynamic resilience of oscillator networks against random perturbations, for a dynamic oscillator model of energy grids. In particular we considered for the topology the two ensembles Erdős-Rényi and small world networks. By using large-deviation methods we were able to measure the distribution of S_m over large ranges of the support, down to small probabilities, which are more difficult or even impossible to access using standard simple sampling, i.e., just repeated simulations. To learn about conditions for high stability, in particular we investigated how S_m correlates with other measurable quantities of power grids or networks.

We found, that for a stable network, a smaller diameter is very preferable, but for smaller stabilities the correlation is not too strong and might be even influenced by the occurrence of the Braess paradox. Also we found that the number of leafs anticorrelates well with a high stability, which corresponds also to the correlation of the size of the two core and of the size of largest biconnected component. Thus tree-like structures should be avoided to create stable grids. Also the universal order parameter, describing the degree of synchronization, should be large and correlates strongly in the range of instable power grids. Furthermore the backup capacity and the power-sign ratio correlate well with the basin stability, supporting the results obtained previously using a large-deviation approach for a static power-flow grid model by investigating the $N-1$ stability.

On the other hand, for the transitivity, we did not find a notable correlation for ER networks and the observed high correlation for SW networks is probably only due to a side effect created by the existence of many long-range links. This leads to small diameters, i.e. high stabilities. The creation of long-range links decreases the number of triangles, which is naturally high in SW networks for small values of the model parameter p.

For further studies, it could be interesting to treat more realistic ensembles of networks, like networks based on two-dimensional real spaces. Furthermore, in the present study only few small perturbations were used to measure the stability. In real modern power grids, not only the consumption, but also the energy productions does constantly and strongly fluctuate. Here, more refined stability measures have to be used, and maybe even to be developed. Also the growth of the importance of renewable energies has to be accompanied by providing more energy storage in grids, which should be considered in models as well. Finally, the dynamic model used here does include only phases, but not amplitudes. Here, the model introduced in Refs. 28 and 29, which is close to the detailed modeling usually done in electrical engineering, could be a good choice. For all these cases, again, by using a large-deviation approach for random ensembles, the most stable and most unstable grids can be explored, to learn about conditions for stable networks.

Finally, it could also be interesting to look at the data from a more mathematical viewpoint, by studying the scaling behavior for different system sizes and obtaining the so called (finite-size) *large-deviation rate function*.[31] If a covergence is observed, this would mean that the distribution has a special finite-size dependence and follows the *large-deviation principle*.

ACKNOWLEDGMENTS

We thank Hendrik Schawe for critically reading the manuscript and him and Hauke Fajen for their valuable discussions. The simulations were performed at the HPC Cluster CARL, located at the University of Oldenburg (Germany) and funded by the DFG through its Major Research Instrumentation Programme (INST 184/157-1 FUGG) and the Ministry of Science and Culture (MWK) of the Lower Saxony State. We also thank the GWDG Göttingen for providing computational resources.

REFERENCES

[1]S. H. Strogatz, *Nonlinear Dynamics and Choas* (Perseus, Cambridge, 2000).
[2]A. Barrat, M. Barthélemy, and A. Vespignani, *Dynamical Processes on Complex Networks* (Cambridge University Press, 2012).
[3]J. Laskar and M. Gastineau, "Existence of collisional trajectories of Mercury, Mars and Venus with the Earth," Nature **459**, 817–819 (2009).
[4]J. C., *Mathematical Modelling in ecology* (Birkenhäuser, Boston, 1989).
[5]R. M. May, "Will a Large Complex System be Stable?" Nature **238**, 413–414 (1972).
[6]A. Becskei and L. Serrano, "Engineering stability in gene networks by autoregulation," Nature **405**, 590—593 (2000).
[7]H. J. Schellnhuber, W. Cramer, N. Nakicenovic, T. Wigley, G. Yohe, T. Blair, and R. Pachauri, *Avoiding Dangerous Climate Change* (Cambridge University Press, Cambridge, 2006).
[8]N. Stern, *The Economics of Climate Change: the Stern Review* (Cambridge University Press, Cambridge, 2007).
[9]M. Timme, L. Kocarev, and D. Witthaut, "Focus on networks, energy and the economy," New Journal of Physics **17**, 110201 (2015).
[10]I. Dobson, B. A. Carreras, V. E. Lynch, and D. E. Newman, "Complex systems analysis of series of blackouts: Cascading failure, critical points, and self-organization," Chaos: An Interdisciplinary Journal of Nonlinear Science **17**, 026103 (2007).
[11]P. Kundur, *Power System Stability and Control* (McGraw-Hill, New York, NY, USA, 1994).
[12]A. E. Motter and Y.-C. Lai, "Cascade-based attacks on complex networks," Phys. Rev. E **66**, 065102 (2002).
[13]A. E. Motter, "Cascade Control and Defense in Complex Networks," Phys. Rev. Lett. **93**, 098701 (2004).
[14]Z. Bao, Y. Cao, L. Ding, and G. Wang, "Comparison of cascading failures in small-world and scale-free networks subject to vertex and edge attacks," Physica A: Statistical Mechanics and its Applications **388**, 4491 – 4498 (2009).
[15]A. K. Hartmann, "Large-deviation properties of resilience of transportation networks," The European Physical Journal B **87**, 114 (2014).
[16]B. Stott, J. Jardim, and O. Alsac, "DC power flow revisited," IEEE Trans. Power Syst. **24**, 1290–1300 (2009).
[17]T. Dewenter and A. K. Hartmann, "Large-deviation properties of resilience of power grids," New Journal of Physics **17**, 015005 (2015).
[18]P. Anderson and A. Fouad, *Power System Control and Stability*, 2nd ed. (IEEE Press, Wiley-Interscience, Piscataway, NJ, USA, 2003).
[19]G. Filatrella, A. H. Nielsen, and N. F. Pedersen, "Analysis of a power grid using a Kuramoto-like model," The European Physical Journal B **61**, 485–491 (2008).
[20]Y. Kuramoto, "Self-entrainment of a population of coupled nonlinear oscillators," in *International Symposium on Mathematical Problems in Theoretical Physics*, edited by H. Araki (Springer Berlin Heidelberg, Berlin, Heidelberg, 1975) pp. 420–422.
[21]M. Rohden, A. Sorge, M. Timme, and D. Witthaut, "Self-Organized Synchronization in Decentralized Power Grids," Phys. Rev. Lett. **109**, 064101 (2012).
[22]H. Magnesius, S. Hirche, and D. Obradovic, in *American Control Conf.* (Fairmont Queen Elizabeth, Montréal, Canada, 2012) p. 2159.
[23]F. Dörfler and F. Bullo, "Synchronization and Transient Stability in Power Networks and Nonuniform Kuramoto Oscillators," SIAM J. Contr. Optim. **50**, 1616–1642 (2012).
[24]D. Witthaut, M. Rohden, X. Zhang, S. Hallerberg, and M. Timme, "Critical Links and Nonlocal Rerouting in Complex Supply Networks," Phys. Rev. Lett. **116**, 138701 (2016).
[25]P. J. Menck, J. Heitzig, J. Kurths, and H. J. Schellnhuber, "How dead ends undermine power grid stability," Nature Communications **5**, 3969 (2014).
[26]F. A. Rodrigues, T. K. D. Peron, P. Ji, and J. Kurths, "The Kuramoto model in complex networks," Physics Reports **610**, 1 – 98 (2016).
[27]P. Ji and J. Kurths, "Basin stability of the Kuramoto-like model in small networks," The European Physical Journal Special Topics **223**, 2483–2491 (2014).
[28]K. Schmietendorf, J. Peinke, R. Friedrich, and O. Kamps, "Self-organized synchronization and voltage stability in networks of synchronous machines," The European Physical Journal Special Topics **223**, 2577–2592 (2014).
[29]K. Schmietendorf, J. Peinke, and O. Kamps, "The impact of turbulent renewable energy production on power grid stability and quality," The European Physical Journal B **90**, 222 (2017).
[30]P. Erdős and A. Rényi, "On the evolution of random graphs," Publ. Math. Inst. Hungar. Acad. Sci **5**, 17–61 (1960).
[31]H. Touchette, "The large deviation approach to statistical mechanics," Physics Reports **478**, 1 – 69 (2009).
[32]J. A. Bucklew, *Introduction to rare event simulation* (Springer-Verlag, New York, 2004).
[33]M. Newman, *Networks: an Introduction* (Oxford University Press, 2010).
[34]M. Brede, "Synchrony-optimized networks of non-identical Kuramoto oscillators," Phys. Lett. A **372**, 2618 – 2622 (2008).
[35]D. Kelly and G. A. Gottwald, "On the topology of synchrony optimized networks of a Kuramoto-model with non-identical oscillators," Chaos: An Interdisciplinary Journal of Nonlinear Science **21**, 025110 (2011).
[36]P. J. Menck, J. Heitzig, N. Marwan, and J. Kurths, "How basin stability complements the linear-stability paradigm," Nature Physics **9**, 89–92 (2013).
[37]C. Mitra, A. Choudhary, S. Sinha, J. Kurths, and R. V. Donner, "Multiple-node basin stability in complex dynamical networks," Phys. Rev. E **95**, 032317 (2017).
[38]J. Nitzbon, P. Schultz, J. Heitzig, J. Kurths, and F. Hellmann, "Deciphering the imprint of topology on nonlinear dynamical network stability," **19**, 033029 (2017).
[39]D. J. Watts and S. H. Strogatz, "Collective dynamics of 'small-world' networks," Nature **393**, 440–442 (1998).
[40]R. E. Belardinelli and V. D. Pereyra, "Fast algorithm to calculate density of states," Phys. Rev. E **75**, 046701 (2007).
[41]F. Wang and D. P. Landau, "Efficient, Multiple-Range Random Walk Algorithm to Calculate the Density of States," Phys. Rev.

Lett. **86**, 2050–2053 (2001).
[42]J. Lee, "New Monte Carlo algorithm: Entropic sampling," Phys. Rev. Lett. **71**, 211–214 (1993).
[43]L. A. N. Amaral, A. Scala, M. Barthélémy, and H. E. Stanley, "Classes of small-world networks," PNAS **97**, 11149–11152 (2000).
[44]A. Barrat and M. Weigt, "On the properties of small-world network models," Eur. Phys. J. B **13**, 547–560 (2000).
[45]J. M. Hammersley and K. W. Morton, "A new Monte Carlo technique: antithetic variates," Math. Proc. Cambr. Phil. Soc. **52**, 449–475 (1956).
[46]C. Dellago, P. G. Bolhuis, F. S. Csajka, and D. Chandler, "Transition path sampling and the calculation of rate constants," J. Chem. Phys. **108**, 1964–1977 (1998).
[47]A. K. Hartmann, "Sampling rare events: statistics of local sequence alignments," Phys. Rev. E **65**, 056102 (2002).
[48]A. Engel, R. Monasson, and A. K. Hartmann, "On the large deviation properties of Erdös-Rényi random graphs," J. Stat. Phys. **117**, 387 (2004).
[49]A. K. Hartmann, "Large-deviation properties of resilience of transportation networks," The European Physical Journal B **87**, 114 (2014).
[50]A. K. Hartmann and M. Mézard, "Distribution of diameters for Erdős-Rényi random graphs," Phys. Rev. E **97**, 032128 (2018).
[51]H. Schawe and A. K. Hartmann, "Large-deviation properties of the largest biconnected component for random graphs," The European Physical Journal B **92**, 73 (2019).
[52]A. K. Hartmann, S. N. Majumdar, and A. Rosso, "Sampling fractional Brownian motion in presence of absorption: A Markov chain method," Phys. Rev. E **88**, 022119 (2013).
[53]A. K. Hartmann, "High-precision work distributions for extreme nonequilibrium processes in large systems," Phys. Rev. E **89**, 052103 (2014).
[54]G. Claussen, A. K. Hartmann, and S. N. Majumdar, "Convex hulls of random walks: Large-deviation properties," Phys. Rev. E **91**, 052104 (2015).
[55]Q. Yan and J. J. de Pablo, "Fast Calculation of the Density of States of a Fluid by Monte Carlo Simulations," Phys. Rev. Lett. **90**, 035701 (2003).
[56]R. E. Belardinelli and V. D. Pereyra, "Nonconvergence of the Wang-Landau algorithms with multiple random walkers," Phys. Rev. E **93**, 053306 (2016).
[57]R. E. Belardinelli, S. Manzi, and V. D. Pereyra, "Analysis of the convergence of the $1/t$ and Wang-Landau algorithms in the calculation of multidimensional integrals," Phys. Rev. E **78**, 067701 (2008).
[58]B. J. Schulz, K. Binder, M. Müller, and D. P. Landau, "Avoiding boundary effects in Wang-Landau sampling," Phys. Rev. E **67**, 067102 (2003).
[59]D. P. Landau, S. Tsai, and M. Exler, "A new approach to Monte Carlo simulations in statistical physics: Wang-Landau sampling," American Journal of Physics **72**, 1294–1302 (2004).
[60]W. H. Press, S. A. Teukolsky, W. T. Vetterling, and B. P. Flannery, *Numerical Recipes 3rd Edition: The Art of Scientific Computing* (Cambridge University Press, 2007).
[61]M. Lakshmanan and S. Rajasekar, *Nonlinear dynamics : integrability, chaos, and patterns*, Advanced texts in physics (Springer, Berlin, 2003).
[62]A. Pikovsky, M. Rosenblum, and J. Kurths, *Synchronization : a universal concept in nonlinear sciences*, Cambridge nonlinear science series 12 (Cambridge Univ. Press, 2001).
[63]C. Runge, "Ueber die numerische Auflösung von Differentialgleichungen," Mathematische Annalen **46**, 167–178 (1895).
[64]W. Kutta, "Beitrag zur näherungsweisen Integration totaler Differentialgleichungen," Zeitschrift für Mathematik und Physik **46**, 435–453 (1901).
[65]J. C. Butcher, "Coefficients for the study of Runge-Kutta integration processes," Journal of the Australian Mathematical Society **3**, 185–201 (1963).
[66]E. Hairer, S. P. Nørsett, and G. Wanner, *Solving Ordinary Differential Equations I: Nonstiff Problems* (Springer Berlin Heidelberg, Berlin, Heidelberg, 1993).
[67]J. C. Butcher, *Numerical methods for ordinary differential equations*, 2nd ed. (Wiley, Chichester, 2008).
[68]M. E. J. Newman, "Scientific collaboration networks. II. Shortest paths, weighted networks, and centrality," Phys. Rev. E **64**, 016132 (2001).
[69]M. G. et al., *GNU Scientific Library Reference Manual* (NETWORK THEORY LTD, Bristol, 2009).
[70]M. Schröder, M. Timme, and D. Witthaut, "A universal order parameter for synchrony in networks of limit cycle oscillators," Chaos: An Interdisciplinary Journal of Nonlinear Science **27**, 073119 (2017).
[71]Y. Kuramoto, *Chemical Oscillations, Waves, and Turbulence* (Springer Berlin Heidelberg, 1984).
[72]S. H. Strogatz, "From Kuramoto to Crawford: exploring the onset of synchronization in populations of coupled oscillators," Physica D: Nonlinear Phenomena **143**, 1 – 20 (2000).
[73]J. Hopcroft and R. Tarjan, "Algorithm 447: Efficient Algorithms for Graph Manipulation," Commun. ACM **16**, 372–378 (1973).
[74]A. Benjamin, G. Chartrand, and P. Zhang, *The fascinating world of graph theory* (Princeton University Press, New Jersey, 2017).
[75]M. E. J. Newman, D. J. Watts, and S. H. Strogatz, "Random graph models of social networks," Proceedings of the National Academy of Sciences **99**, 2566–2572 (2002).
[76]B. Bollobás and O. M. Riordan, "Mathematical results on scale-free random graphs," in *Handbook of Graphs and Networks* (John Wiley & Sons, Ltd, 2005) Chap. 1, pp. 1–34.
[77]T. Schank and D. Wagner, "Approximating Clustering Coefficient and Transitivity," Journal of Graph Algorithms and Applications **9**, 265–275 (2005).
[78]A. K. Hartmann and M. Weigt, *Phase Transitions in Combinatorial Optimization Problems* (Wiley-VCH, Weinheim, 2005).
[79]M. E. J. Newman and G. T. Barkema, *Monte Carlo Methods in Statistical Physics* (Oxford University Press, 1999).
[80]D. Braess, "Über ein Paradoxon aus der Verkehrsplanung," Unternehmensforschung **12**, 258–268 (1968).
[81]D. Witthaut and M. Timme, "Braess's paradox in oscillator networks, desynchronization and power outage," New Journal of Physics **14**, 083036 (2012).